Arginine 66 Controls Dark-State Formation in Green-to-Red Photoconvertible Fluorescent Proteins

Romain Berardozzi, Virgile Adam, Alexandre Martins, Dominique Bourgeois

JACS
JOURNAL OF THE AMERICAN CHEMICAL SOCIETY
Article
pubs.acs.org/JACS

Arginine 66 Controls Dark-State Formation in Green-to-Red Photoconvertible Fluorescent Proteins

Romain Berardozzi, Virgile Adam,* Alexandre Martins, and Dominique Bourgeois*

†Institut de Biologie Structurale, Université Grenoble Alpes, CEA, CNRS, 38044 Grenoble, France

Supporting Information

ABSTRACT: Photoactivated localization microscopy (PALM) is a powerful technique to investigate cellular nanostructures quantitatively and dynamically. However, the use of PALM for molecular counting or single-particle tracking remains limited by the propensity of photoconvertible fluorescent protein markers (PCFPs) to repeatedly enter dark states. By designing the single mutants mEos2-A69T and Dendra2-T69A, we completely swapped the blinking behaviors of mEos2 and Dendra2, two popular PCFPs. We combined X-ray crystallography and single-molecule microscopy to show that blinking in mEos2 and Dendra2 is largely controlled by the orientation of arginine 66, a highly conserved residue in Anthozoan PCFPs. The Arg66 side-chain conformation affects the bleaching and the *on*-to-*off* transition quantum yields, as well as the fraction of molecules entering long-lived dark states, resulting in widely different apparent blinking behaviors that largely modulate the efficiency of current blinking correction procedures. The present work provides mechanistic insight into the complex photophysics of Anthozoan PCFPs and will facilitate future engineering of bright and low-blinking variants suitable for PALM.

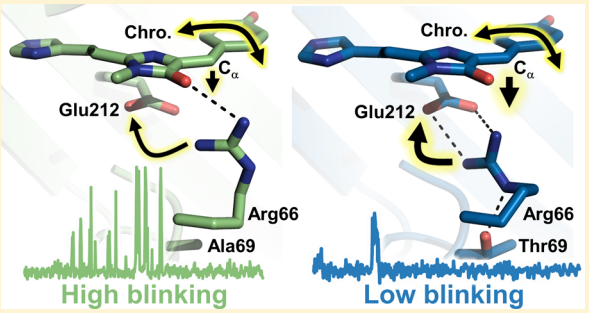

INTRODUCTION

Green-to-red photoconvertible fluorescent proteins (PCFPs) have become popular markers to investigate cellular structures at the nanoscale with photoactivated localization microscopy (PALM).[1,2] Beyond standard PALM-based applications with fixed or live cells, PCFPs are employed in advanced applications such as a quantitative PALM (q-PALM), to measure protein copy-number or stoichiometry at the single-molecule level,[3] or single-particle tracking PALM (spt-PALM), to extract diffusion traces from a large pool of target molecules.[4] However, the pronounced tendency of PCFPs to transiently enter dark states (i.e., to "blink") complicates the use of PALM, notably to investigate cellular nanostructures quantitatively and dynamically. Indeed, a photoconverted (red) PCFP experiencing multiple blinking cycles before irreversible bleaching may be confounded with multiple non-blinking molecules, causing clusterization artifacts in super-resolved images and counting errors in q-PALM.[5] In spt-PALM, the accurate tracking of highly mobile target molecules is complicated by prolonged dark periods of the PCFP labels, during which molecular trajectories are lost.[6] Photoblinking affects all fluorescent proteins (FPs) and was first reported in green fluorescent protein (GFP) variants.[7] Blinking photophysics in FPs have been studied by fluorescence correlation spectroscopy (FCS),[8−12] steady-state,[13,14] time-resolved,[14,15] single-molecule,[16−20] structural,[21] and theoretical[12,22,23] approaches, and have been found to span a wide range of time scales from fast (∼1−100 kHz)[8−11] to slow (∼0.1−10 Hz).[16,17,24] Changes in chromophore protonation, isomeric state, or spin state have been proposed to be responsible for photoblinking,[25] but a detailed understanding of blinking mechanisms in FPs is currently lacking.

Blinking can be somewhat reduced by controlling the PCFP's nanoenvironment,[18,26] but this is generally not a viable strategy in live cells. A number of sophisticated algorithms have been proposed to correct for blinking in PALM data,[18,19,27−29] but the efficiency of these procedures drops abruptly when the labeling density increases, or, importantly, when the *on*-state recovery rate decreases. Recovery rates below 1 s^{-1}, typically observed in all PCFPs for a fraction of the molecules, are thus particularly difficult to deal with.

The successful design of "low-blinking" PCFPs would constitute an important breakthrough for PALM-based applications. However, the difficulty in setting up efficient screening protocols to assess blinking properties[15] renders the use of directed-evolution approaches challenging, and rather prompts at engineering efforts based on rational design. Hence, gaining more mechanistic insight into the photophysics of PCFP's blinking is desirable.

Our earlier work on IrisFP, a PCFP derived from EosFP that displays, in addition to photoconversion, reversible photoswitching properties in both its green and red states,[30] suggested the existence of a radical-based transient dark state in which the C_α atom of the chromophore methylene bridge adopts a sp^3 configuration, giving rise to a distorted, nonfluorescent chromophore.[22,31] Crystallographic data and quantum chem-

Received: September 21, 2015
Published: December 17, 2015

DOI: 10.1021/jacs.5b09923
J. Am. Chem. Soc. 2016, 138, 558−565

ical/molecular mechanical calculations suggested that Arg66, a highly conserved residue in PCFPs of Anthozoan origin, located in the close vicinity of the chromophore, might directly influence this blinking behavior by transiently donating a proton to the C_α atom. Moreover, Arg66 was proposed to play a possible role in photobleaching, notably through photo-oxidative pathways involving decarboxylation of the conserved Glu212.[22,32−34]

Interestingly, Dendra2 and mEos2, two of the most popular PCFPs in which Arg66 adopts different conformations,[21,35] display significantly different blinking and bleaching behaviors.[19,20] In mEos2, like in IrisFP, Arg66 interacts with the carbonyl group of the chromophore imidazolinone ring. *In vitro* immobilized mEos2 displays a high propensity to blink, is relatively resistant to photobleaching, and an important fraction of mEos2 dark states are long-lived.[19] Conversely, Dendra2, in which Arg66 interacts with the glutamate 212, exhibits a relatively low propensity to blink, is poorly resistant to photobleaching, and its dark states are mainly short-lived.[19] These differences, however, appear to be modulated by the sample-specific nano-environment.[18,20]

Previous work has shown that it is possible to control the conformation of Arg66 through substitution of the residue at position 69, which, depending on its nature, may or may not interact with Arg66.[21,36] This strategy was used to demonstrate that the orientation of Arg66 in EosFP,[21] Dendra2,[21] and pcDronpa[36] tunes the electron density pattern along the chromophore in both the ground and excited states, resulting in shifts of the excitation/emission maxima and protonation equilibrium (pK_a). Here, to isolate the influence of the Arg66 conformation on blinking and bleaching in mEos2 and Dendra2, we designed the single mutants mEos2-A69T and Dendra2-T69A and performed combined single-molecule and crystallographic measurements. The results highlight the profound influence of Arg66 in controlling the entire photophysical behavior of Anthozoan PCFPs and provide general insight into the molecular mechanisms of dark-state formation in these essential markers.

EXPERIMENTAL PROCEDURES

Experimental procedures are described in detail in the Supporting Information.

RESULTS

Steady-State Spectroscopy. As expected, the single substitution of the alanine at position 69 by a threonine turns mEos2 into a Dendra2-like emitter by inducing a hypsochromic shift of the absorption and fluorescence emission maxima and by stabilizing the protonated chromophore for both the green and red forms (Table S1, Figures S1−S4). Likewise, the reverse mutation T69A turns Dendra2 into a mEos2-like emitter (Table S1, Figures S1−S4). The Dendra2-T69A chromophore resides mainly in its anionic fluorescent form at physiological pH, leading to an increased rate of photon emission compared to its parent Dendra2.

***In Vitro* Single-Molecule Measurements Using a Novel Immobilization Assay.** In order to investigate the blinking behavior of mEos2, Dendra2 and their respective variants, we developed a single-molecule assay. FPs were immobilized by covalent cross-linking of their N termini and solvent-exposed amine groups (lysine and arginine residues) to a glass coverslide functionalized with (3-aminopropyl)triethoxysilane (APTES) and disuccinimidyl suberate (DSS) (Figure 1A; see Supporting Information for details). This new method allows immobilization of any molecule carrying free amine functions without requiring any particular fixation tag such as biotine, while allowing full control of environmental conditions (oxygen content, redox conditions, and pH among others) by simply changing the mounting medium. This method allows recording of single-molecule fluorescence time traces with high signal-to-noise ratio (Figure 1B) while potentially avoiding adverse effects linked to matrix embedding.[37] Agreement between photophysical parameters measured on mEos2 and Dendra2 using either a biotin/streptavidin immobilization assay[19] or our method suggests a neutral effect of DSS anchoring on FPs' photophysics.

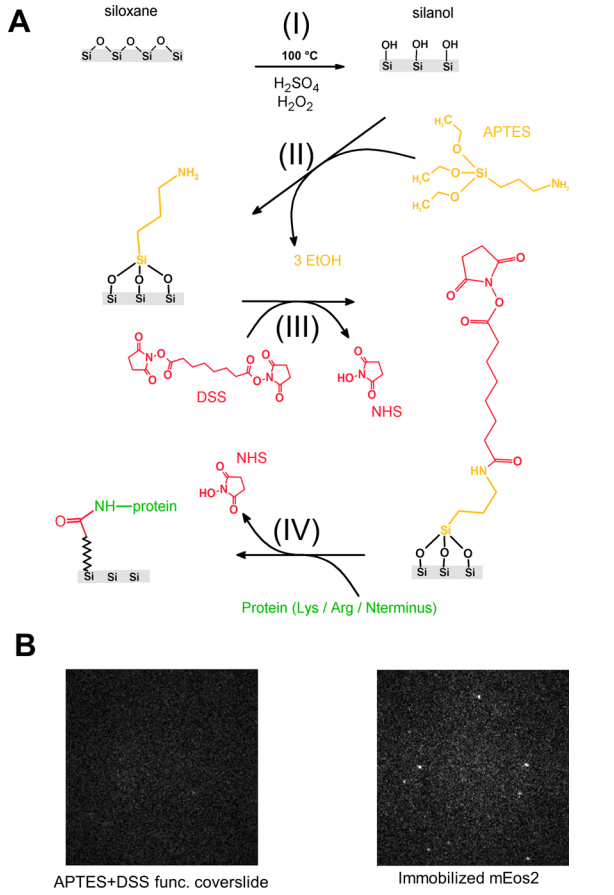

Figure 1. (A) Scheme of the functionalization method used to immobilize single molecules by means of double covalent bonding. (B) Functionalized coverslides devoid of mEos2 show no red fluorescence contamination (left). In the presence of photoconverted mEos2, fluorescence from immobilized single molecules can be identified (right). (Images are displayed on the same intensity scale.)

Figure 2A shows characteristic kymograms and fluorescence time traces of immobilized single-molecules in a PBS pH 7.4 buffer. Dendra2 and mEos2-A69T show a low tendency to blink before irreversible bleaching. In contrast, Dendra2-T69A and mEos2 show a marked tendency to blink with short *on*-times punctuated by several *off*-times before bleaching. The change in brightness caused by the single-substitutions at position 69 also appears evident. To precisely assess the effect of the A69T and T69A mutations on the blinking and bleaching behavior of mEos2 and Dendra2, we measured the average number of blinks experienced by a molecule, as well as the macroscopic blinking/

DOI: 10.1021/jacs.5b09923
J. Am. Chem. Soc. 2016, 138, 558−565

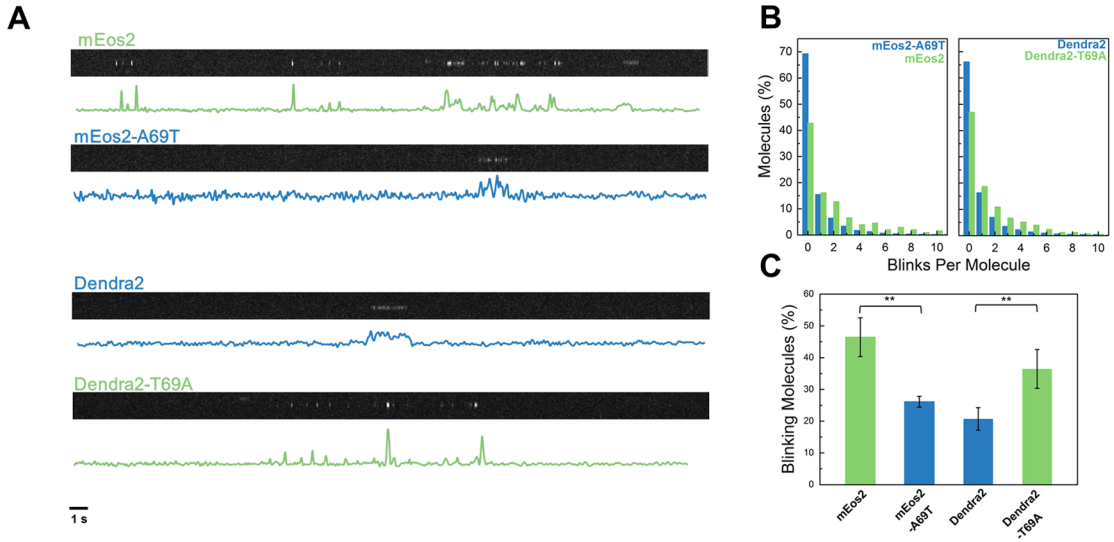

Figure 2. Blinking behavior of *in vitro* immobilized mEos2, Dendra2 and their respective variants. (A) Characteristic kymograms and fluorescence time traces of single-molecules. (B) Histograms of the number of blinks experienced by single-molecules. (C) Fraction of molecules that experience at least one blinking event during their lifetime. Data shown as mean ± standard deviation of triplicate experiments. *p-value ≤0.05, **p-value ≤0.01 obtained for two-independent-samples t-tests.

Table 1. Blinking and Bleaching Properties of Immobilized mEos2, Dendra2, and Their Respective Variants Measured *in Vitro* (PBS, pH 7.4) in Their Photoconverted Red Form

	mEos2	mEos2-A69T	Dendra2	Dendra2-T69A
photon budget[a]	$(10 \pm 1) \times 10^2$	$(4.4 \pm 0.2) \times 10^2$	$(4.7 \pm 0.7) \times 10^2$	$(7 \pm 0.5) \times 10^2$
average blinks per molecule[b]	0.93 ± 0.2	0.39 ± 0.04	0.29 ± 0.05	0.62 ± 0.2
fraction of blinking molecules (%)	46 ± 6	26 ± 1	21 ± 3	36 ± 6
bleaching macroscopic rate (s^{-1})[c]	8.9 ± 0.2	16.4 ± 3.7	21.4 ± 2.6	15.8 ± 3.0
blinking macroscopic rate (s^{-1})[c]	8.2 ± 0.8	6.3 ± 0.9	6.2 ± 0.5	9.7 ± 0.7
bleaching quantum yield[d]	$(1.1 \pm 0.2) \times 10^{-5}$	$(5.3 \pm 1.2) \times 10^{-5}$	$(5.0 \pm 0.6) \times 10^{-5}$	$(1.5 \pm 0.3) \times 10^{-5}$
blinking quantum yield[d]	$(1.0 \pm 0.1) \times 10^{-5}$	$(2.0 \pm 0.2) \times 10^{-5}$	$(1.4 \pm 0.1) \times 10^{-5}$	$(9.0 \pm 0.6) \times 10^{-6}$
fast blinking quantum yield[d]	$(2.4 \pm 0.5) \times 10^{-6}$	$(9.2 \pm 0.2) \times 10^{-6}$	$(5.2 \pm 0.8) \times 10^{-6}$	$(2.4 \pm 0.6) \times 10^{-6}$
slow blinking quantum yield[d]	$(7.6 \pm 0.8) \times 10^{-6}$	$(1.08 \pm 0.2) \times 10^{-5}$	$(8.8 \pm 0.8) \times 10^{-6}$	$(6.5 \pm 0.6) \times 10^{-6}$
bleaching microscopic rate (s^{-1})[e]	$(2.7 \pm 0.5) \times 10^3$	$(12.6 \pm 0.3) \times 10^3$	$(11.4 \pm 0.1) \times 10^3$	$(3.5 \pm 0.7) \times 10^3$
blinking microscopic rate (s^{-1})[e]	$(2.4 \pm 0.2) \times 10^3$	$(4.7 \pm 0.4) \times 10^3$	$(3.1 \pm 0.2) \times 10^3$	$(2.1 \pm 0.1) \times 10^3$
fast blinking microscopic rate (s^{-1})[e]	$(0.58 \pm 1.3) \times 10^3$	$(2.2 \pm 0.4) \times 10^3$	$(1.2 \pm 0.2) \times 10^3$	$(0.58 \pm 1.5) \times 10^3$
slow blinking microscopic rate (s^{-1})[e]	$(1.8 \pm 0.2) \times 10^3$	$(2.5 \pm 0.4) \times 10^3$	$(2.0 \pm 0.2) \times 10^3$	$(1.5 \pm 0.1) \times 10^3$
slow recovery rate (s^{-1})[f]	1.2 ± 0.1	1.4 ± 1.6	1.7 ± 0.9	1.6 ± 0.2
fast recovery rate (s^{-1})[f]	16.8 ± 2.1	18.6 ± 4.6	15.7 ± 3.7	15.7 ± 4.5
fraction of long-lived dark states (%)	76 ± 2	54 ± 8	63 ± 4	73 ± 5

[a]Photon budget is calculated as the number of photons detected during the lifetime of the protein. [b]Average number of blinks is calculated as the ratio between blinking and bleaching rates (k_d/k_{bl}). [c]Macroscopic bleaching rates are calculated by fitting the bleach-time histograms with a monoexponential model (see Figure S7 and Experimental Procedures for details). Macroscopic blinking rates are estimated from *on*-time histograms after correcting for the contribution of bleaching. [d]Blinking and bleaching quantum yields are derived from the measured macroscopic rates after correcting for laser power density, laser wavelength, and molar extinction coefficients of red chromophores (as reported in Table S1). Slow and fast blinking quantum yields are calculated as $\varphi_{blink,slow} = \varphi_{blink} f_{long}$ and $\varphi_{blink,fast} = \varphi_{blink}(1 - f_{long})$, respectively, with φ_{blink} the blinking quantum yield and f_{long} the fraction of long-lived dark states. [e]Microscopic rates are calculated as the ratio between phototransformation's quantum yields and excited state lifetimes (see Table S1). [f]Slow and fast recovery rates are obtained by fitting the *off*-time histograms with a double-exponential model (Figure 4A and Figure S7). Values are given as mean ± standard deviation from triplicate experiments.

bleaching rates based on the analysis of single-molecule fluorescence time traces retrieved with a refined version of the method proposed by Lee et al.[18,19]

The single-substitutions A69T in mEos2 and T69A in Dendra2 essentially swap the blinking propensities of the two PCFPs (Figure 2B,C). The average number of blinks per molecule in mEos2 (0.93) drops by a factor of 2.4 in the A69T mutant (Table 1). Accordingly, the fraction of mEos2-A69T molecules that experience blinking is reduced by a factor of 1.8 (26% vs 46% for mEos2). In contrast, the single substitution T69A in Dendra2 increases the average number of blinks experienced by a molecule by a factor of 2.1 and the fraction of blinking molecule by a factor of 1.6. Interestingly, while Dendra2-T69A displays an overall photophysical behavior similar to that of mEos2 (Table S1), it is fully monomeric at high concentration (Figure S5), whereas mEos2 is known to dimerize.[35]

The observed number of blinks of a FP, as shown in Figure 2, is dictated by both its reversible dark-state conversion and its irreversible bleaching kinetics ($\langle N_{blink} \rangle = k_d/k_{bl}$, with k_d the dark-

DOI: 10.1021/jacs.5b09923
J. Am. Chem. Soc. 2016, 138, 558−565

state-conversion and k_{bl} the bleaching rates[19]). We measured k_d and k_{bl} for Dendra2, mEos2, and their respective mutants by fitting the *on*-time and bleach-time histograms reconstructed from the single-molecule fluorescence time traces (Figure S6), according to the kinetic model presented in Figure S7. The single-substitution A69T in mEos2 results in a 1.8-fold increase in the bleaching rate and a 1.3-fold decrease in the dark-state-conversion rate (Figure 3A,B, Table 1). In contrast, the

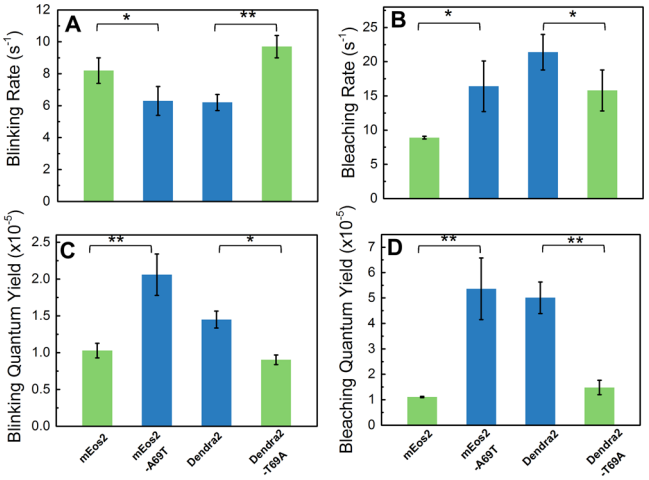

Figure 3. Blinking (A) and bleaching (B) rates measured for *in vitro* immobilized mEos2, Dendra2 and their respective variants. Blinking (C) and bleaching (D) quantum yields retrieved after correcting for local laser power densities and molar extinction coefficients of the anionic red forms at the excitation wavelength (reported in Table S1). Data shown as mean ± standard deviation of triplicate experiments. *p-value ≤0.05, **p-value ≤0.01 obtained for two-independent-samples t-tests.

Dendra2-T69A mutant displays a 1.3 times decrease in the bleaching rate and a 1.6-fold increase in the dark-state-conversion rate (Figure 3A,B, Table 1). Correcting for the excitation rates, which depend on local laser power density and extinction coefficients at the excitation wavelength (Table S1), the quantum yields of bleaching and dark-state-conversion can be estimated (for details see ref 18). Due to the large differences in extinction coefficients, which mostly result from substantial deviations in chromophore pK_as, it appears that the bleaching quantum yields of Dendra2 and mEos2-A69T largely exceed those of mEos2 and Dendra2-T69A and that, more surprisingly, their dark-state-conversion quantum yields also stand above, although to a lower extent (Table 1, Figure 3C,D). The reduced observed number of blinks in Dendra2 and mEos2-A69T relative to mEos2 and Dendra2-T69A thus results from strongly increased bleaching, not from reduced conversion to reversible dark states.

Next, we analyzed the *off*-time distributions of the four PCFP variants. As shown by others,[19,38] the *off*-time histograms are well fitted by a double-exponential model, suggesting the existence of two dark states characterized by different lifetimes (Figure 4A, Figure S8). The data show that mEos2 and Dendra2-T69A enter more frequently into long-lasting dark states (76% and 73% of the blinking population, respectively) compared to mEos2-A69T and Dendra2 (54% and 63% of the population, respectively) (Figure 4B, Table 1). The *on*-state recovery rates do not significantly vary between all variants (Figure S8A), suggesting that the same dark states are populated and that their thermodynamics is not strongly affected by the

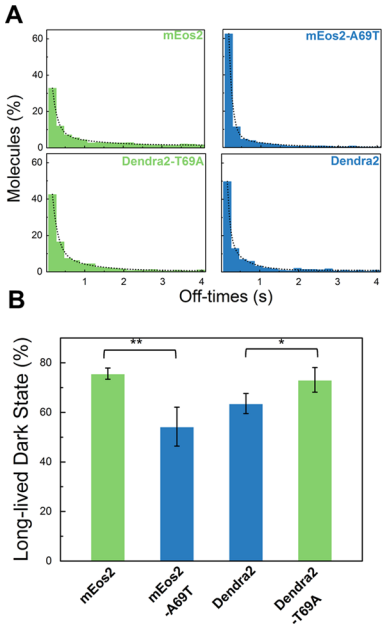

Figure 4. Behavior of dark-state populations of *in vitro* immobilized mEos2, Dendra2, and their respective variants. (A) *Off*-time distributions fitted by a double-exponential model represented as black dotted lines. (B) Fractions of blinking molecules entering a long-lived dark state. Data shown as mean ± standard deviation of triplicate experiments. *p-value ≤0.05, **p-value ≤0.01 obtained for two-independent-samples t-tests.

orientation of Arg66. Furthermore, in agreement with previous reports,[19] we found that only the slow recovery rate is influenced by 405 nm light (Figure S8B). Taking into account the fraction of molecules that enter short and long-lived dark states, respectively, the quantum yields for fast and slow blinking can be obtained (Table 1).

To relate our single-molecule data with the bulk behavior of our PCFPs, we performed additional measurements at the ensemble level. In the case of mEos2 and Dendra2-T69A, the data clearly suggest that a large fraction of the population enters a dark state that recovers on the several minutes to seconds time scale in the absence or presence of 405 nm light, respectively (Figure S9). For Dendra2 and mEos2-A69T, in contrast, a lower fraction of the population enters a dark state, with similar recovery rates in the presence of 405 nm light.

The data are thus consistent with the ensemble-level dark state corresponding to the long-lived dark state evidenced at the single-molecule level. The lower amount of recovery observed in Figure S9 for Dendra2 and mEos2-A69T also fully agrees with photobleaching being higher in the case of these two variants. However, the ensemble data are not consistent with the magnitude of the photobleaching quantum yields measured at the single-molecule level. Considering the large difference in laser excitation intensities used in ensemble and single-molecule experiments, this finding is in line with a nonlinear photobleaching mechanism that depends on the subsequent absorption of two photons.

In order to get further insights into the blinking and bleaching mechanisms, we investigated their sensitivity to the local nanoenvironment, which can be conveniently performed using our immobilization assay. We characterized the photophysical behavior of our PCFPs at the single-molecule level in anaerobic conditions using a glucose/glucose oxidase/catalase O_2-

DOI: 10.1021/jacs.5b09923
J. Am. Chem. Soc. 2016, 138, 558−565

scavenging system, and in a strong oxidizing environment using $Fe(CN)_6$. For both conditions, a significant drop in the signal-to-noise ratio of the data was noticed for all variants. The bleaching quantum yield of mEos2 in the absence of oxygen was found significantly increased compared to normal oxygenated conditions (Figure S10). This suggests that under the strong illumination conditions used in PALM, bleaching mainly occurs through an oxygen-independent mechanism likely to involve the triplet state, the lifetime of which is increased in the absence of O_2. Consistently, in the presence of $Fe(CN)_6$, the bleaching quantum yield strongly increased, highlighting the sensitivity of the chromophore to redox-driven photochemistry. In parallel, the fraction of mEos2 molecules experiencing fast blinking relative to slow blinking was found increased in both anaerobic and oxidative conditions. These findings are consistent with fast blinking also involving triplet state redox chemistry, while slow blinking could be triggered by conformational dynamics occurring in the singlet excited state. Similar findings were found for all variants (Figure S10).

***In Cellulo* Single-Molecule Measurements.** To assess the effect of the cellular environment, we performed single-molecule measurements on fixed HeLa cells expressing mEos2, Dendra2, or their respective variants free in the cytoplasm. Arg66 was found to control the mean number of blinks, the rates of bleaching and dark-state conversion, and the fraction of molecules entering the long-lived dark state in a similar manner as was found *in vitro* (Table S2, Figures S11 and S12). Despite rather strong variability between individual measurements, which we attribute to intercellular heterogeneity, a tendency for increased bleaching was noticed, when compared to the *in vitro* results. This could result from the redox-active cytoplasmic environment.

Crystallographic Studies. In order to get insights into how Arg66 controls the bleaching and blinking mechanisms at play in the studied PCFPs, we solved the crystallographic structure of mEos2-A69T (green form, PDB access code: 5DTL) and compared it to those of mEos2 (PDB access code: 3S05) and Dendra2 (PDB access code: 2VZX). The structure of mEos2-A69T confirms that the single mutation on residue 69 was sufficient to transform the chromophore environment of mEos2 into the one of Dendra2 (Figure 5). In mEos2, Arg66 adopts a stretched conformation toward the chromophore in which the guanidinium moiety interacts with the carbonyl group of the imidazolinone ring while standing 6.5 Å away from the carboxyl group of Glu212. The distance between the N_η atoms and the chromophore C_α atom is ~3.5 Å (Figure 5, Table 2). This distance shrinks to ~3.2 Å for $N_{\eta 1}$ in a model inspired from blinked IrisFP[31] in which the chromophore is placed in a distorted sp^3 geometry (Figure 5B, Table 2). In comparison, in Dendra2 and mEos2-A69T, the conformation adopted by the Arg66 side chain is curled, as a result of the interaction between the hydroxyl group of Thr69 and the ε-amine of the guanidinium moiety (Figure 5C,E). Consequently, the $N_{\eta 1}$ atom now forms a salt bridge with the carboxyl group of Glu212. In this conformation the guanidinium does not interact with the imidazolinone carbonyl of the chromophore but points directly below the methylene bridge so that the distance between atom $N_{\eta 1}$ of Arg66 and atom C_α of the chromophore shrinks from ~3.5 to <2.9 Å in a putative distorted blinked state, largely below the distance measured for mEos2 (Figure 5D,F). Overall, in Dendra2 and mEos2-A69T, Arg66 appears to be in a more favorable position to promote decarboxylation of Glu212 and to donate a proton to the C_α atom in a coupled electron-/proton-transfer process.[22] We note that although these conclusions derive from crystallographic structures obtained in the green states of the PCFPs, they are expected to remain valid in the red states, as green-to-red photoconversion is known to imply only very minor structural reorganization around the chromophore, and thus does not substantially modify the Arg66 interaction pattern.[2]

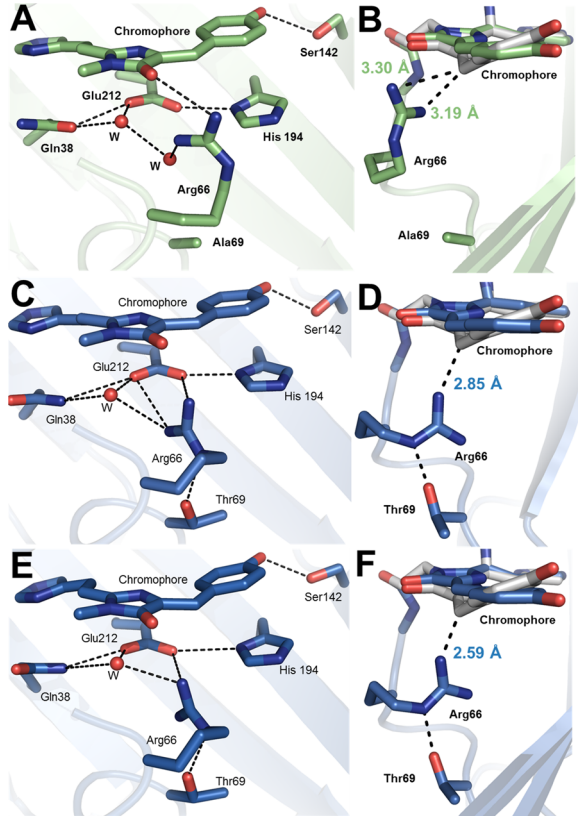

Figure 5. Crystallographic structures of mEos2 (A,B), Dendra2 (C,D), and mEos2-A69T. (E,F) Hydrogen bonds are represented as black dotted lines. Distorted chromophores (light gray in B, D, and F) are attributed to a short-lived dark state. The geometry of the distorted chromophores was taken from the X-ray structure of an IrisFP short-lived dark state (PDB access code: 3TMT[22]) and chromophore alignments were performed by least-squares minimization.

Table 2. Distances (Å) between Key Atoms Involved in Bleaching and Blinking, from Crystallographic Structures

	mEos2	mEos2-A69T	Dendra2
N_η^{Arg66}–C=O^{chromophore}	3.12	4.15	3.88
N_η^{Arg66}–C=O^{Glu212}	5.8	3.3	3.17
N_η^{Arg66}–C–O^{-} ^{Glu212}	6.54	3.97	3.83
N_η^{Arg66}–$C_\alpha^{planar\ chromophore}$	3.45	3.54	3.48
N_η^{Arg66}–C_α IrisFP distorted chromophore[a]	3.19/3.30[b]	2.85	2.59

[a]The reported distances may be underestimated due to the structural response of the FP scaffold to the distortion of the chromophore in the short-lived dark state. [b]For mEos2, Arg66 adopts a conformation in which N_η^1 and N_η^2 stand close to the benzylidene carbon in the distorted state, while in mEos2-A69T and Dendra2, the curled-up conformation allows an interaction between the benzylidene carbon and only one out of the two N_η.

Design of mEos2-R66L. In a quest for low-blinking and photostable PCFP variants, we sought to design a mEos2 mutant in which the nature of the residue at position 66 would avoid any electrostatic interaction and proton exchange with

DOI: 10.1021/jacs.5b09923
J. Am. Chem. Soc. 2016, 138, 558–565

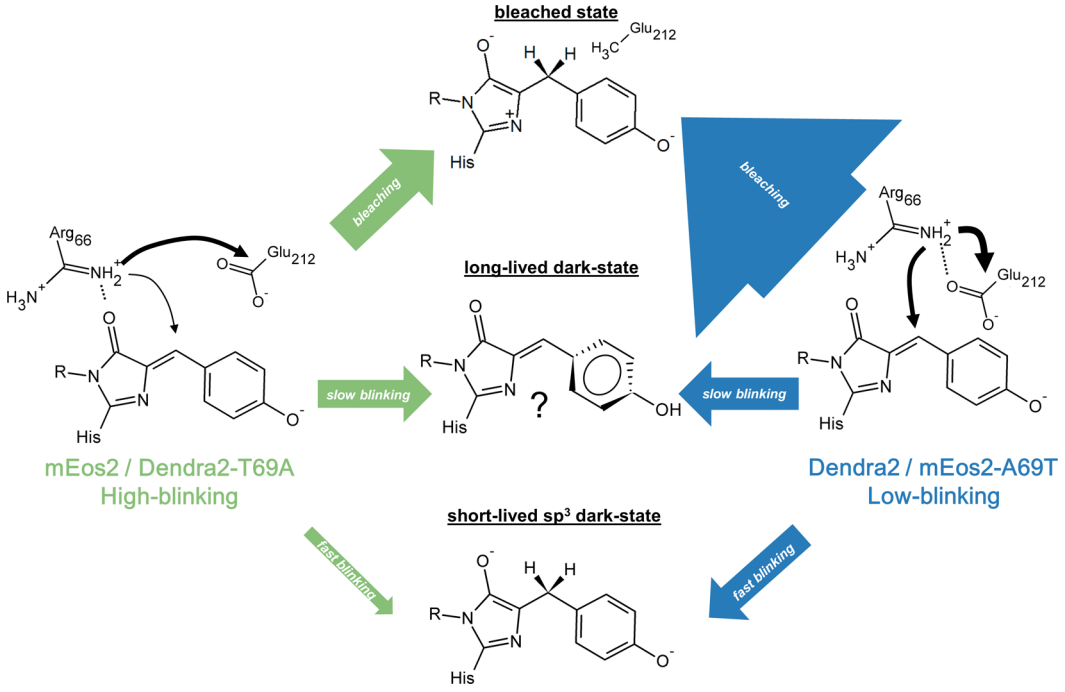

Figure 6. Proposed phototransformations in mEos2-like and Dendra2-like PCFPs. The thickness of the arrows reflects the measured microscopic rates of the considered phototransformations. Black arrows are indicative of proton transfers.

either the chromophore or Glu212. The almost isosteric variant mEos2-R66L could be successfully engineered but the chromophore was found mainly protonated at pH 7.4 and did not show detectable photoconversion to a red form under 405-nm illumination (Figure S13). Moreover, in its green form, this variant showed a pronounced photochromic behavior under alternating illumination with 488- and 405-nm light, similarly to the mGeos[39]or Skylan-S[40] variants (Figure S13). These data show that Arg66, in addition to blinking and bleaching, also plays an essential role in green-state photoswitching and in green-to-red photoconversion, suggesting that mutating this residue is unlikely to be a viable strategy to rationally engineer improved PCFPs.

DISCUSSION

The combined analysis of the single-molecule and crystallographic data reveals how the single residue Arg66 precisely controls blinking and bleaching in Anthozoan PCFPs and provides insight into the associated molecular mechanisms. Notably, quantitative analysis of the single-molecule fluorescence traces allows extracting the quantum yields of the studied phototransformations in the experimental conditions of localization microscopy. Microscopic rates can then be obtained as $k = \phi/\tau$, with ϕ the quantum yield and τ the excited-state lifetime. These microscopic rates, reported in Table 1, provide an absolute measure of the propensity to enter a given phototransformation pathway. Hence, they provide general guidelines for a fair mechanistic comparison between our four variants (Figure 6).

The much higher microscopic bleaching rate of Dendra2 and mEos2-A69T as compared to Dendra2-T69A and mEos2 (>220% increase) strongly suggests that the orientation of Arg66 controls the bleaching mechanism. Our findings are consistent with the hypothesis that Arg66 favors Glu212 decarboxylation when its guanidinium group directly interacts with this residue through a salt bridge. In IrisFP, Glu212 decarboxylation has been shown to be a dominant photobleaching pathway under high-intensity laser illumination (~kW/cm^2), as typically employed in single-molecule localization microscopy. This mechanism is oxygen independent and involves the triplet state as a starting point, in line with the increased bleaching we observed in mEos2 under anaerobic conditions. Glu212 decarboxylation in FPs has been proposed to proceed from the carboxylate conjugate form of the glutamate[41] through a Kolbe-like photoreaction that involves a $^{\bullet}CH_2$ radical intermediate[22,33,42] followed by protonation to form a final methyl group. In Dendra2 and mEos2-A69T, the strong saline interaction between the positively charged Arg66 and the Glu212 likely results in a stabilization of the conjugate base of the carboxylic acid function carried by the glutamate, accounting for the higher microscopic bleaching rates. Moreover, the electrophilic Arg66 guanidinium moiety may also favor Glu212 decarboxylation via an electron-withdrawing effect that would result in a weakening of the C_γ–C_δ bond. In addition, Arg66 could provide the final proton to the $^{\bullet}CH_2$ species, as it does to the C_α atom in case of blinking, as described above.[22] Interestingly, such scenario is corroborated by the higher photoresistance of mOrange relative to its parent DsRed, in which the conformation of the amine-carrying residue Lys70 (66 in PCFPs) is not interacting anymore with Glu215 (212 in PCFPs).[24,34]

The higher propensity of Dendra2 and mEos2-A69T to switch from the *on* state to the short-lived dark state, compared to Dendra2-T69A and mEos2 (>100% increase), together with the crystallographic observation of a reduced distance between Arg66 and atom C_α of the putatively distorted chromophore, strongly suggest that the short-lived dark state corresponds to a radical-based chromophore in which the C_α atom is protonated and sp^3-hybridized. This is further substantiated by our observation that recovery from the short-lived dark state is not accelerated by 405-nm light illumination (Figure S8B), in line with the distorted state in IrisFP not absorbing visible

DOI: 10.1021/jacs.5b09923
J. Am. Chem. Soc. 2016, 138, 558–565

light.[31] In such a mechanism, the shorter distance in Dendra2 and mEos2-A69T between the N_η atom of Arg66 and atom C_α of the chromophore would favor proton tunneling in a coupled electron-/proton-transfer pathway.[22] Furthermore, such a redox-based mechanism, also proposed to involve the triplet state as a starting point,[22] would not be discouraged in anaerobic conditions, as observed.

The long-lived dark state responds to stimulation by 405-nm light and is thus assigned to a hydroxy-phenol protonated state of the chromophore. The percent changes in the propensity of Dendra2 and mEos2-A69T to switch to this state, relative to Dendra2-T69A and mEos2 are relatively moderate (+33% and +38% increase in rates, respectively), suggesting that Arg66 does not play a major role in the associated mechanism. The limited accuracy of our phototransformation quantum yields resulting from potential residual systematic errors in the determination of the molar extinction coefficients in the red state of PCFPs indeed prevents us to consider the observed changes significant. A first candidate for the long-lived dark state could be the *trans* protonated form of the chromophore. However, several arguments argue against this hypothesis. First, it has been reported for Dronpa that the *trans* isomer of the chromophore is more likely populated if the Arg66 and the imidazolinone ring interact, as it does in mEos2, by favoring single bond τ-rotation.[43] Time-resolved Fourier transform infrared spectroscopy (FTIR) revealed a weakening of the Arg66-imidazolinone bond during *cis*−*trans* isomerization, explaining why Arg66 can easily lose interaction with the chromophore in the *trans* state.[44] Second, the presence of an interaction between Arg66 and Thr69, as in Dendra2, has been proposed to reduce formation of the *trans* isomer in monomeric Azami Green (mAG).[45] In such curled conformation, Arg66 stands closer to His194 that thus gets clogged due to stronger van der Waals interactions, limiting chromophore isomerization. Thus, if our long-lived dark state would correspond to a *trans* chromophore, we would expect significantly higher microscopic rates for mEos2 and Dendra2-T69A, contrary to our findings. Furthermore, *trans* chromophore conformations in reversibly switchable FPs are typically highly stable, with lifetimes up to many hours in the dark, at variance with our ensemble-level experiments.

The above-mentioned observations lead us to attribute slow blinking in our PCFP variants to a protonated *cis* or twisted state. As the planar *cis* protonated form is expected to live for only microseconds,[8,25] a yet-uncharacterized twisted ground-state protonated form appears more likely. Such a form could possibly be reached via twisted internal charge transfer (TICT) involving rotation around the chromophore phenoxy exocyclic C−C bond. The importance of TICT pathways, and their coupling with chromophore protonation has been recognized in several studies.[46−48] Due to the lack of interaction between Arg66 and the imidazolinone carbonyl moiety in Dendra2 and mEos2-A69T, a more pronounced single-bond character of the phenoxy bond is expected in these variants, favoring engagement into a phenoxy TICT channel and consistent with the relative microscopic rates we measured. Moreover, a phenyl twisted conformer of the chromophore may relax to a ground state predicted to be long-lived.[47] Importantly, twisting through TICT channels is strongly governed by the electronic nature of the chromophore surrounding, and again the different Arg66 orientations in our variants could play an important role in this respect, similarly to what has been proposed in the chromoprotein Phanta and its variants.[49] Finally, a long-lived dark state reached through a TICT channel would be consistent with a singlet, rather than triplet, excited-state process, in line with our data. Nevertheless, further experimental and theoretical investigations are needed to test this proposal.

CONCLUSION

We have shown that the conserved amino acid Arg66 controls the entire range of photophysical properties in Anthozoan PCFPs: brightness, photoconversion, photoblinking and photobleaching. Exchanging the conformation of Arg66 in mEos2 and Dendra2, which only share 72.2% sequence identity, is sufficient to completely swap the photophysical behaviors of these two PCFPs. Thus, the reason for which mEos2 is currently preferred for applications requiring high photon counts, whereas Dendra2 is better suited for molecular counting or tracking experiments can be essentially related to the different conformations of Arg66.

In the course of this work, we have also introduced a simple *in vitro* single-molecule immobilization assay based on disuccinimidyl suberate cross-linking that allows full control of the physicochemical environment while avoiding the need for any protein engineering. Another outcome of this study is the design of Dendra2-T69A. This variant combines the high photon budget of mEos2 with the fully natural monomeric character of Dendra2. As natural monomers have been found preferable to engineered monomers,[50] Dendra2-T69A could advantageously replace mEos2 or possibly even its advanced variants[35] in applications requiring maximized photon output but in which the latter PCFPs affect fusion gene functionality.

This work provides insight into photobleaching and blinking mechanisms in green-to-red photoconvertible FPs of Anthozoan origin. Under the laser illumination conditions used in localization microscopy, Glu212 decarboxylation appears to be a main pathway for redox-induced photobleaching.[33,41] Chromophore distortion and twisting are likely candidates for short-lived and long-lived dark-state formation, respectively. Further comparative studies with other recently developed PCFPs[35,36,51,52] and possibly in live cells should be performed to confirm these hypotheses and provide an even more refined picture of the complex blinking and bleaching mechanisms at play in these smart labels. Engineering of bright and low-blinking PCFPs displaying efficient green-to-red photoconversion is likely to be challenged by the central role of Arg66. Dendra2-T69A could nevertheless be a favorable starting template. Mutations increasing the steric hindrance or altering the electrostatic potential around the phenoxy moiety of the chromophore in order to reduce phenoxy ring twisting should be envisaged to design optimized variants for counting and tracking purpose.

ASSOCIATED CONTENT

Supporting Information

The Supporting Information is available free of charge on the ACS Publications website at DOI: 10.1021/jacs.5b09923.

Experimental methods and material on single-molecule data acquisition and processing, crystal growth, X-ray data collection, and structure determination, including Tables S1−S3 and Figures S1−S13 (PDF)

AUTHOR INFORMATION

Corresponding Authors

*virgile.adam@ibs.fr

*dominique.bourgeois@ibs.fr

DOI: 10.1021/jacs.5b09923
J. Am. Chem. Soc. 2016, 138, 558−565

Notes

The authors declare no competing financial interest.

■ ACKNOWLEDGMENTS

This work used the platforms of the Grenoble Instruct Centre (ISBG; UMS 3518 CNRS-CEA-UJF-EMBL) with support from FRISBI (ANR-10-INSB-05-02) and GRAL (ANR-10-LABX-49-01) within the Grenoble Partnership for Structural Biology (PSB). Support for this work comes from the Agence Nationale de la Recherche (ANR-2011-BSV5-012-01 NOBLEACH). We thank Christine Ebel and Aline LeRoy for ultracentrifugation analysis and Michel Sliwa (LASIR, Université Lille 1) for his precious help in measuring the excited-state lifetimes.

■ REFERENCES

(1) Sengupta, P.; van Engelenburg, S. B.; Lippincott-Schwartz, J. *Chem. Rev.* **2014**, *114*, 3189.
(2) Adam, V.; Berardozzi, R.; Byrdin, M.; Bourgeois, D. *Curr. Opin. Chem. Biol.* **2014**, *20*, 92.
(3) Sengupta, P.; Jovanovic-Talisman, T.; Lippincott-Schwartz, J. *Nat. Protoc.* **2013**, *8*, 345.
(4) Manley, S.; Gillette, J. M.; Lippincott-Schwartz, J. *Methods Enzymol.* **2010**, *475*, 109.
(5) Annibale, P.; Vanni, S.; Scarselli, M.; Rothlisberger, U.; Radenovic, A. *Nat. Methods* **2011**, *8*, 527.
(6) Lane, L. A.; Smith, A. M.; Lian, T.; Nie, S. *J. Phys. Chem. B* **2014**, *118*, 14140.
(7) Dickson, R. M.; Cubitt, A. B.; Tsien, R. Y.; Moerner, W. E. *Nature* **1997**, *388*, 355.
(8) Haupts, U.; Maiti, S.; Schwille, P.; Webb, W. W. *Proc. Natl. Acad. Sci. U. S. A.* **1998**, *95*, 13573.
(9) Heikal, A. A.; Hess, S. T.; Baird, G. S.; Tsien, R. Y.; Webb, W. W. *Proc. Natl. Acad. Sci. U. S. A.* **2000**, *97*, 11996.
(10) Liu, Y.; Kim, H. R.; Heikal, A. A. *J. Phys. Chem. B* **2006**, *110*, 24138.
(11) Schenk, A.; Ivanchenko, S.; Rocker, C.; Wiedenmann, J.; Nienhaus, G. U. *Biophys. J.* **2004**, *86*, 384.
(12) Vegh, R. B.; Bravaya, K. B.; Bloch, D. A.; Bommarius, A. S.; Tolbert, L. M.; Verkhovsky, M.; Krylov, A. I.; Solntsev, K. M. *J. Phys. Chem. B* **2014**, *118*, 4527.
(13) Sinnecker, D.; Voigt, P.; Hellwig, N.; Schaefer, M. *Biochemistry* **2005**, *44*, 7085.
(14) McAnaney, T. B.; Zeng, W.; Doe, C. F.; Bhanji, N.; Wakelin, S.; Pearson, D. S.; Abbyad, P.; Shi, X.; Boxer, S. G.; Bagshaw, C. R. *Biochemistry* **2005**, *44*, 5510.
(15) Manna, P.; Jimenez, R. *J. Phys. Chem. B* **2015**, *119*, 4944.
(16) David, C. C.; Dedecker, P.; De Cremer, G.; Verstraeten, N.; Kint, C.; Michiels, J.; Hofkens, J. *Photochem. Photobiol. Sci.* **2012**, *11*, 358.
(17) Annibale, P.; Scarselli, M.; Kodiyan, A.; Radenovic, A. *J. Phys. Chem. Lett.* **2010**, *1*, 1506.
(18) Avilov, S.; Berardozzi, R.; Gunewardene, M. S.; Adam, V.; Hess, S. T.; Bourgeois, D. *PLoS One* **2014**, *9*, e98362.
(19) Lee, S. H.; Shin, J. Y.; Lee, A.; Bustamante, C. *Proc. Natl. Acad. Sci. U. S. A.* **2012**, *109*, 17436.
(20) Durisic, N.; Laparra-Cuervo, L.; Sandoval-Alvarez, A.; Borbely, J. S.; Lakadamyali, M. *Nat. Methods* **2014**, *11*, 156.
(21) Adam, V.; Nienhaus, K.; Bourgeois, D.; Nienhaus, G. U. *Biochemistry* **2009**, *48*, 4905.
(22) Roy, A.; Field, M. J.; Adam, V.; Bourgeois, D. *J. Am. Chem. Soc.* **2011**, *133*, 18586.
(23) Vegh, R. B.; Bloch, D. A.; Bommarius, A. S.; Verkhovsky, M.; Pletnev, S.; Iwai, H.; Bochenkova, A. V.; Solntsev, K. M. *Phys. Chem. Chem. Phys.* **2015**, *17*, 12472.
(24) Shaner, N. C.; Lin, M. Z.; McKeown, M. R.; Steinbach, P. A.; Hazelwood, K. L.; Davidson, M. W.; Tsien, R. Y. *Nat. Methods* **2008**, *5*, 545.
(25) Moerner, W. E. *J. Phys. Chem. B* **2002**, *106*, 910.
(26) Vogelsang, J.; Cordes, T.; Forthmann, C.; Steinhauer, C.; Tinnefeld, P. *Proc. Natl. Acad. Sci. U. S. A.* **2009**, *106*, 8107.
(27) Lando, D.; Endesfelder, U.; Berger, H.; Subramanian, L.; Dunne, P. D.; McColl, J.; Klenerman, D.; Carr, A. M.; Sauer, M.; Allshire, R. C.; Heilemann, M.; Laue, E. D. *Open Biol.* **2012**, *2*, 120078.
(28) Annibale, P.; Vanni, S.; Scarselli, M.; Rothlisberger, U.; Radenovic, A. *PLoS One* **2011**, *6*, e22678.
(29) Coltharp, C.; Kessler, R. P.; Xiao, J. *PLoS One* **2012**, *7*, e51725.
(30) Adam, V.; Lelimousin, M.; Boehme, S.; Desfonds, G.; Nienhaus, K.; Field, M. J.; Wiedenmann, J.; McSweeney, S.; Nienhaus, G. U.; Bourgeois, D. *Proc. Natl. Acad. Sci. U. S. A.* **2008**, *105*, 18343.
(31) Adam, V.; Carpentier, P.; Violot, S.; Lelimousin, M.; Darnault, C.; Nienhaus, G. U.; Bourgeois, D. *J. Am. Chem. Soc.* **2009**, *131*, 18063.
(32) Adam, V.; Moeyaert, B.; David, C. C.; Mizuno, H.; Lelimousin, M.; Dedecker, P.; Ando, R.; Miyawaki, A.; Michiels, J.; Engelborghs, Y.; Hofkens, J. *Chem. Biol.* **2011**, *18*, 1241.
(33) Duan, C.; Adam, V.; Byrdin, M.; Ridard, J.; Kieffer-Jaquinod, S.; Morlot, C.; Arcizet, D.; Demachy, I.; Bourgeois, D. *J. Am. Chem. Soc.* **2013**, *135*, 15841.
(34) Fron, E.; Van der Auweraer, M.; Moeyaert, B.; Michiels, J.; Mizuno, H.; Hofkens, J.; Adam, V. *J. Phys. Chem. B* **2013**, *117*, 2300.
(35) Zhang, M.; Chang, H.; Zhang, Y.; Yu, J.; Wu, L.; Ji, W.; Chen, J.; Liu, B.; Lu, J.; Liu, Y.; Zhang, J.; Xu, P.; Xu, T. *Nat. Methods* **2012**, *9*, 727.
(36) Moeyaert, B.; Nguyen Bich, N.; De Zitter, E.; Rocha, S.; Clays, K.; Mizuno, H.; van Meervelt, L.; Hofkens, J.; Dedecker, P. *ACS Nano* **2014**, *8*, 1664.
(37) Piwonski, H.; Sokolowski, A.; Waluk, J. *J. Phys. Chem. Lett.* **2015**, *6*, 2477.
(38) Rollins, G. C.; Shin, J. Y.; Bustamante, C.; Presse, S. *Proc. Natl. Acad. Sci. U. S. A.* **2015**, *112*, E110.
(39) Chang, H.; Zhang, M.; Ji, W.; Chen, J.; Zhang, Y.; Liu, B.; Lu, J.; Zhang, J.; Xu, P.; Xu, T. *Proc. Natl. Acad. Sci. U. S. A.* **2012**, *109*, 4455.
(40) Zhang, X.; Chen, X.; Zeng, Z.; Zhang, M.; Sun, Y.; Xi, P.; Peng, J.; Xu, P. *ACS Nano* **2015**, *9*, 2659.
(41) Ding, L.; Chung, L. W.; Morokuma, K. *J. Phys. Chem. B* **2013**, *117*, 1075.
(42) van Thor, J. J.; Gensch, T.; Hellingwerf, K. J.; Johnson, L. N. *Nat. Struct. Biol.* **2002**, *9*, 37.
(43) Li, X.; Chung, L. W.; Mizuno, H.; Miyawaki, A.; Morokuma, K. *J. Phys. Chem. Lett.* **2010**, *1*, 3328.
(44) Warren, M. M.; Kaucikas, M.; Fitzpatrick, A.; Champion, P.; Sage, J. T.; van Thor, J. J. *Nat. Commun.* **2013**, *4*, 1461.
(45) Ebisawa, T.; Yamamura, A.; Kameda, Y.; Hayakawa, K.; Nagata, K.; Tanokura, M. *Acta Crystallogr., Sect. F: Struct. Biol. Cryst. Commun.* **2010**, *66*, 485.
(46) Altoe, P.; Bernardi, F.; Garavelli, M.; Orlandi, G.; Negri, F. *J. Am. Chem. Soc.* **2005**, *127*, 3952.
(47) Drobizhev, M.; Hughes, T. E.; Stepanenko, Y.; Wnuk, P.; O'Donnell, K.; Scott, J. N.; Callis, P. R.; Mikhaylov, A.; Dokken, L.; Rebane, A. *Sci. Rep.* **2012**, *2*, 688.
(48) Olsen, S.; Smith, S. C. *J. Am. Chem. Soc.* **2007**, *129*, 2054.
(49) Don Paul, C.; Traore, D. A.; Olsen, S.; Devenish, R. J.; Close, D. W.; Bell, T. D.; Bradbury, A.; Wilce, M. C.; Prescott, M. *PLoS One* **2015**, *10*, e0123338.
(50) Yu, D.; Baird, M. A.; Allen, J. R.; Howe, E. S.; Klassen, M. P.; Reade, A.; Makhijani, K.; Song, Y.; Liu, S.; Murthy, Z.; Zhang, S. Q.; Weiner, O. D.; Kornberg, T. B.; Jan, Y. N.; Davidson, M. W.; Shu, X. *Nat. Methods* **2015**, *12*, 763.
(51) Paez-Segala, M. G.; Sun, M. G.; Shtengel, G.; Viswanathan, S.; Baird, M. A.; Macklin, J. J.; Patel, R.; Allen, J. R.; Howe, E. S.; Piszczek, G.; Hess, H. F.; Davidson, M. W.; Wang, Y.; Looger, L. L. *Nat. Methods* **2015**, *12*, 215.
(52) McEvoy, A. L.; Hoi, H.; Bates, M.; Platonova, E.; Cranfill, P. J.; Baird, M. A.; Davidson, M. W.; Ewers, H.; Liphardt, J.; Campbell, R. E. *PLoS One* **2012**, *7*, e51314.

DOI: 10.1021/jacs.5b09923
J. Am. Chem. Soc. 2016, 138, 558−565